

Charting the Realms of Mesoscale Cloud Organisation using Unsupervised Learning

L. Denby^{1,2}

¹Danish Meteorological Institute, Copenhagen, DK

²University of Leeds, UK

Key Points:

- The internal representation of an unsupervised-trained neural network forms a map of all possible states of trade wind shallow cloud organisation
- Mesoscale organisation does affect shortwave albedo even when correcting for changes in cloud-fraction
- By capturing the continuum of organisation, this cloud map enables the study of the temporal evolution of organisation

Abstract

Quantifying the driving mechanisms and effect on Earth’s energy budget of mesoscale cloud organisation remains difficult, in part because quantifying the organisational state of the atmosphere through an objective means remains a challenge. We present the first technique to map the full continuum of convective organisation states by extracting the manifold of the internal representation used by a neural network trained through unsupervised learning. By compositing reanalysis and remote sensing observations onto this manifold, we are able to quantify how wind-speed and water vapour concentration are key environmental characteristics associated with changes in organisation. Using the manifold we place distinct organisational regimes, defined in prior work, into the full continuum of organisation. We quantify for the first time, how mesoscale shallow cloud organisation affects Earth’s albedo in the tropics besides simply changing the cloud-fraction; changes in cloud-optical depth produce changes in albedo in the range of $\pm 1.4\%$ in addition to what would be predicted from cloud-fraction alone¹. And, finally we demonstrate how using the continuum representation of this manifold technique enables analysis of the temporal evolution of cloud organisation. The presented manifold of mesoscale cloud organisation provides a novel means to quantify cloud organisation, enabling the study of mechanisms behind transitions between regimes (in simulations and observations) by capturing the full continuum of organisational regimes. This will enable future work to quantify how well models of atmospheric flow capture mesoscale cloud organisation, in turn paving the way for better representation of cloud organisation in simulations of Earth’s climate.

1 Introduction

From satellite imagery of Earth it is immediately clear that clouds often organise into spatial patterns. Names have been given to the most prominent patterns we recognise (e.g. fronts, cyclones, cellular cloud-decks, etc) and we use this classification to study the impacts of clouds on Earth’s weather and climate through their precipitation and interaction with radiation and atmospheric circulation.

¹ In the final stages of preparing this manuscript we became aware of independent, related work by (Alinaghi et al., 2023)

One particular form of clouds, shallow tradewind cumuli, have a profound importance in Earth’s climate system due to their ubiquity and net cooling effect, stemming from these clouds reflecting more incoming short-wave radiation from the sun compared to the outgoing long-wave radiation they permit (Bony et al., 2004). Differing predictions of how these clouds will respond to a warming climate accounts for most of the variation in climate sensitivity between climate models (Bony & Dufresne (2005), Webb et al. (2006), Medeiros et al. (2008), Vial et al. (2013)), which highlights the urgent need to better understand how these clouds form and interact with their environment (one of the World Climate Research Programme’s Grand Science Challenges, Bony et al. (2015)).

One particular aspect of shallow convective clouds that is still poorly understood, is their mesoscale organisation, both in quantifying what regimes occur, the driving mechanisms behind them and extent to which mesoscale cloud organisation impacts Earth’s climate. This interest in convective organisation stems from the observation that in high-resolution (Large Eddy) simulations, clouds cluster (self-aggregate) under certain conditions (Wing et al., 2018; Muller et al., 2022), which results in a change in cloud-fraction and net radiation for the same domain-mean state. Given the necessarily coarse resolution of climate models ($O(10\text{km})$), neither the processes driving organisation nor the organisational regimes can be explicitly resolved and so the behaviour of these shallow clouds (and their radiative impact) must be parameterised.

In the context of the EUREC⁴A field campaign (Stevens et al., 2021) work by Stevens et al. (2019) [S19] developed a set of four classifications for shallow cloud organisation by manual examination of visual satellite imagery. These classes were motivated by the physical processes expected important in different regimes, and have since formed the framing for many studies investigating the conditions under which different forms of organisation occur, both in observations (Bony et al., 2020; Schulz et al., 2021) [B21, S21] and in simulations (Dauhut et al., 2023), with particular focus on the transition from small to larger isolated detraining shallow clouds (Narenpitak et al., 2021a; Saffin et al., 2023a).

An alternative approach was taken by Denby (2020) [D20] who developed an unsupervised machine learning approach to autonomously discover the possible states of mesoscale organisation without imposing specific classes. This approach of unsupervised learning was also taken by Kurihana, Foster, et al. (2022); Kurihana, Moyer, Willett, et

al. (2022); Kurihana, Moyer, & Foster (2022) using clustering to produce individual classes of cloud patterns. Differently again, Janssens et al. (2021) [J21] utilised the framework of traditional metrics used for measuring clouds and their organisation (rather imposing specific classes), concluding that rather than occurring in isolated regimes, cloud organisation exists in a continuum (at least when viewed through these metrics).

By building on D20 we will demonstrate in this work how the continuum of convective organisation states is captured as an emergent property of the internal *embedding space* representation, learnt by a neural network through unsupervised learning. Specifically, we will extract the low-dimensional manifold within the high-dimensional embedding space on which all possible states of convective organisation lie, and explore this manifold through the metrics and classes of [J21] and [S19]. Through composition of re-analysis and observations onto this manifold we characterise environmental conditions vary with convective organisation, we quantify the effect of organisation on radiation correcting for changes in cloud-fraction, and further demonstrate how transitions between organisational states can be studied with the manifold.

2 Methods

The primary tool used in this work is a convolutional neural network which takes as input a 2D image-tile containing cloud imagery (derived here from satellite observations) and produces a point in a high-dimensional *embedding space* (here 100-dimensional, as in [D20]), a so-called *embedding vector*. During training the neural network has learnt to place tiles with similar cloud structures nearby in the embedding space. This is achieved by training the network on contrastive tile triplets of similar and dissimilar cloud-patterns (produced by sampling from satellite imagery both spatially closely-overlapping *anchor-neighbor* and randomly distributed *distant* tiles).

The image-tiles utilised here were generated by performing locally planar projections of observations from the geostationary GOES-16 satellite to produce 256×256 pixel input tiles spanning $200\text{km} \times 200\text{km}$. In extension to D20's use of truecolor RGB-composite tiles, we here also generate a set of tiles using the three *water-vapour window* infrared channels (11, 14 & 15) and train a separate IR-tiles model. This enables characterisation of convective organisation throughout the diurnal cycle (including nighttime), enabling analysis of cloud evolution over multiple days (see subsection 3.6).

We use the Level-2 $\Delta x \approx 4\text{km}$ 1-hourly CERES radiation products derived from the GOES-16 geostationary satellite (NASA/LARC/SD/ASDC, 2018) (NASA/LARC/SD/ASDC, 2017, produces similar but smaller albedo variations due to its coarser resolution). Environmental characteristics associated with different states of organisation were extracted by resampling ERA5 reanalysis (Hersbach et al., 2020) onto the dataset tiles. For cloud-fraction and cloud metric calculations (Denby & Janssens, 2022) we use the shallow cloud-mask as defined by (Bony et al., 2020), thresholding on GOES-16 channel 13 ($10.35\mu\text{m}$) brightness temperature ($280K < T_b^{ch13} < 290K$). To aid comparison with prior work we have chosen to restrict our analysis to tiles with minimum cloud top-temperature above freezing level $T_c > 273K$.

3 Results

3.1 The manifold of mesoscale cloud organisation

In this section we will demonstrate how the continuum of cloud organisation states can be extracted as an emergent property of the embedding space utilised by a trained neural network. We do this by examining the topological structure of the embeddings produced by the neural network applied to a dataset of 10,000 triplet tiles.

As the neural network has learnt during training to place similar cloud structures close in the embedding space, the occurrence of evolution between organisation states will manifest as a continuum of points in the embedding space (assuming a dataset large enough to contain the in-between states). The extent to which this point-cloud maps out isolated regions, clusters connected by isolated paths, or full manifolds of smooth evolution, tells us not only what kinds of regimes exist, but also how distinct they are and what transitions between regimes are actually observed in nature. Prior work by [S19] suggests that organisation in the tropical Atlantic comes in four distinct forms, which would manifest as the embeddings lying in four isolated clusters. However, clustering analysis shows no evidence of isolated clusters in the embedding space. Indeed, should we expect the atmosphere to gravitate to only few distinct forms of cloud organisation? If the atmosphere is constantly evolving between different forms of organisation, why would it stay "stuck" in specific isolated regimes of organisation rather than spending as much time transitioning between regimes? Since attempts to find isolated clusters failed, we moved to techniques which are able to maintain the continuum representation that em-

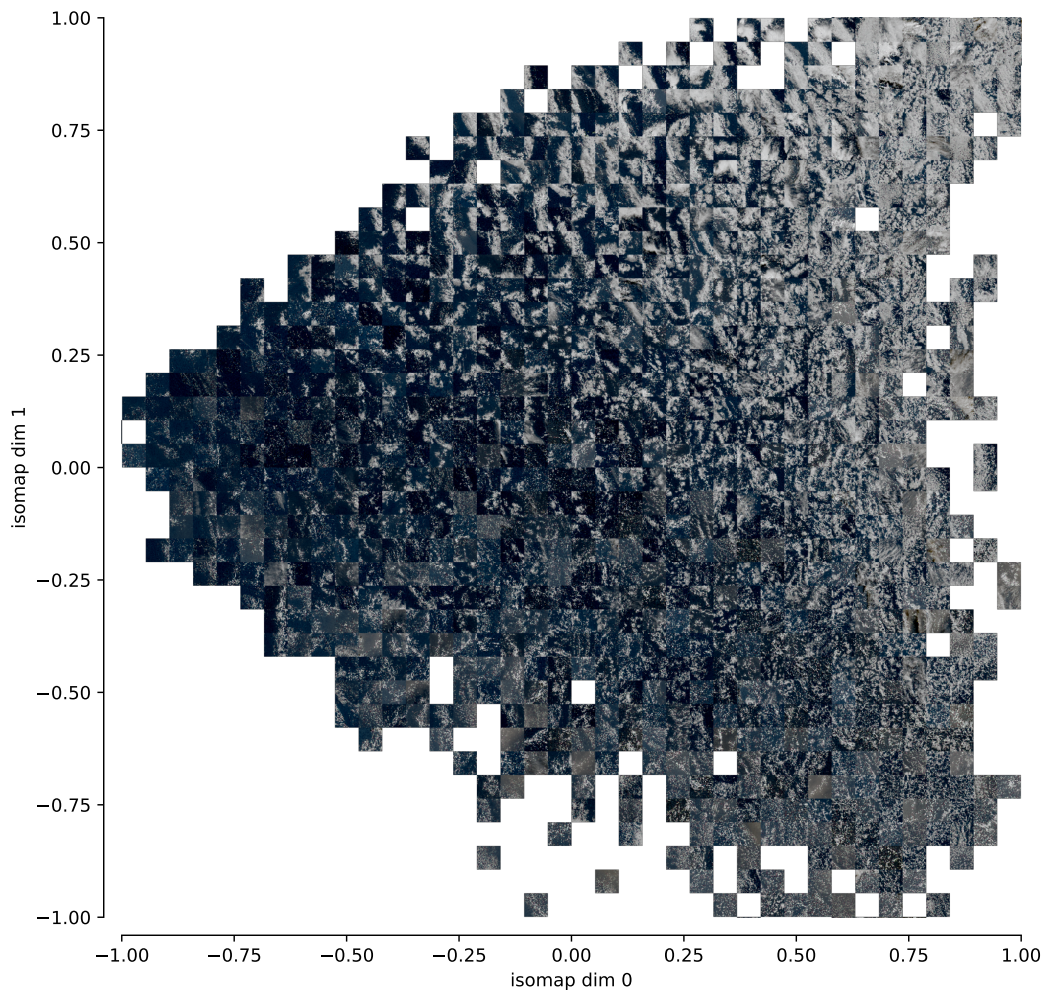


Figure 1: Convective organisation embedding manifold visualised by the anchor tile from the closest anchor-neighbour pair within a fixed interval across the manifold

bedding vectors of organisation provide. By applying manifold extraction techniques to the embedding space we found that the tile embeddings do indeed appear to lie on a low-dimensional manifold within the high-dimensional embedding space.

We applied the Isomap Tenenbaum et al. (2000) manifold extraction method to transform the 100D embedding-vector point cloud into a 2D plane, the result of which is visualised in Figure 1 by rendering tiles for individual points across the manifold. Isomap was selected because it through construction of a nearest-neighbour graph through the entire tile embedding point-cloud, ensures that the topology of the manifold is unchanged (i.e. does not introduce or remove new paths between points). The manifold extraction allows us to perform dimensionality reduction of the embedding space, by extracting only the part of the embedding space that the neural network has actually utilised. Using a manifold extraction method, rather than for example Principal Component Analysis (PCA), avoids assuming that the embedding points lie on a high-dimensional plane since Isomap follows the curvature of the manifold spanned by the tile embedding points.

To visualise the embedding manifold select the closest anchor-neighbor pair for each fixed-width bin across the embedding manifold, and render the anchor tile from that pair (Figure 1). This produces tiles with a clearly discernable pattern by exploiting that where the trained neural network is unable to place two anchor-neighbor tiles in close proximity (in the embedding space), this suggests that either a) these tiles are very different in the cloud structures present (unlikely given the spatial overlap of anchor-neighbor tiles) or b) it is not possible for the neural network to characterise the organisational state of these two tiles and so these tiles are not in a clearly discernable organisational state. Conversely, closely-spaced anchor-neighbor tiles are not only similar, but in an organisational state clearly identifiable by the trained neural network.

We can by eye immediately identify differences in the morphological features of clouds in different parts of the manifold, with smaller isolated clouds concentrated in the lower left, larger isolated clouds in the upper corner and the bottom right populated by cellular cloud structures. Having produced this 2D "map" of cloud organisation through extraction of the underlying manifold utilised by the neural network, we turn in the next sections to examining the organisational states spanned within this manifold, both in terms of properties of the clouds and their environment and through the effects of organisation on radiation. This is done by aggregating observations and reanalysis datasets (co-

incident in time and space with the sampled tiles) onto the 2D manifold by binning each physical variable in turn by the 2D manifold dimensions. For each variable we will consider the mean for each bin, the variance and standard error in the mean are included in the supplementary material.

3.2 Cloud-metrics on manifold

In this section we will set the embedding manifold extracted in subsection 3.1 in a more familiar context by computing the set of four cloud property metrics identified by J21 as collectively being able to describe the majority of variation between organisational regimes: a) the cloud length-scale (L_c), b) open-sky amount (f_{os} , Antonissen, 2019), c) directional anisotropy (WOI_3) of liquid water path (a_{LWP} , Brune et al., 2021) and d) standard deviation of cloud-top height (σ_{CTH}). In addition, we include the common cloud characteristics of e) cloud-fraction f_c and f) cloud-top height z_{CTH} . The variation of these metrics across the embedding manifold is shown in the respective subfigures of Figure 2, which depict the mean value for each variable across all tiles falling within a given bin in on 2D manifold.

Visually, it is immediately clear that using just these metrics there are many ways to split up the embedding manifold into regions of similar characteristics, with both smooth and abrupt changes in the cloud property metrics across the manifold. As cloud-size is a very familiar characteristic that relates to how a cloud was formed and the radiative impact it has, we will concentrate on separately examining the large regions of the manifold where the characteristic cloud-size remains near-constant. For the very smallest clouds ($L_c < 20\text{km}$ in Figure 2a) the principal variation is the decrease in the characteristic open-sky amount (Figure 2b) with increasing cloud-top height (Figure 2f) (and lesser increase in cloud-fraction, Figure 2e), which describes the transition from scattered isolated clouds (left in the manifold) to more cellular (cold-pool arc) cloud formations (bottom right of the manifold). The largest clouds ($L_c > 20\text{km}$) are found in more varied configurations; specifically, with either a) very variable cloud-top height (Figure 2d), intermediate cloud-fraction and large regions of open-sky (the large isolated clouds in the top left of the manifold), but also situations b) with less variation in cloud-top height and lower cloud-fraction (the top right of the manifold).

It is worth pausing here to consider how a 2D plane appears to be adequate to map all regimes of the shallow cumulus organisation when J21 showed that a full set off four metrics are needed. We, conjecture that this is principally because J21 used PCA and so explicitly assumed that variations in mesoscale organisation can be described by a set of linear basis defined by the metrics used. However, as noted by J21 it is not clear that the linear decomposition is physically meaningful for cloud organisation, evidenced by the metrics not being linearly separable. Said differently, it is quite possible that the full set of four metrics are only required to distinguish a subset of organisational states and for other regimes the metrics actually covary. We see this behaviour in our analysis as the first two metrics (L_c and f_{os}) show an unidirectional gradient across the entire embedding manifold, whereas the last two metrics, a_{LWP} and σ_{CTH} (Figure 2c and 2d) primarily vary within smaller regions where the first two metrics are near-constant.

The extent to which the space of possible organisational states is indeed inherently two-dimensional, will be investigated using topological analysis tools in future work. However, through the compositing cloud and environment characteristics (the latter in the next section) on the 2D embedding manifold we do find physically meaningful interpretations of variability observed and so we expect that to leading order the 2D manifold here is a useful tool to understanding what kinds of organisation form and why they form.

3.3 Environmental characteristics of mesoscale organisation

Next we will examine how the environment varies with different forms of organisation by compositing ERA5 reanalysis on the embedding manifold. Across the manifold we will quantify how organisation varies with environmental characteristics (Figure 3) and contrast these relationships with findings in prior work.

In agreement with B21 and S21, in conditions with the lowest wind-speeds (Figure 3a and 3a) and relatively warm sea-surface temperatures (Figure 3f), we find the archetypical scattered shallow cumuli and in conditions with lowest sea-surface temperature and highest wind-speeds, the shallow more cellular cloud structures formed by evaporation-driven cold-pools (these forms of organisation are also called *Sugar* and *Gravel*, see subsection 3.4). Contrasting the manifold regions with the smallest (and shallowest, $z_{CTH} < 2km$) and largest (and deepest, $z_{CTH} \approx 4km$) isolated clouds we find that the environmental factor which most clearly differentiates these regions to be sub-cloud and cloud-

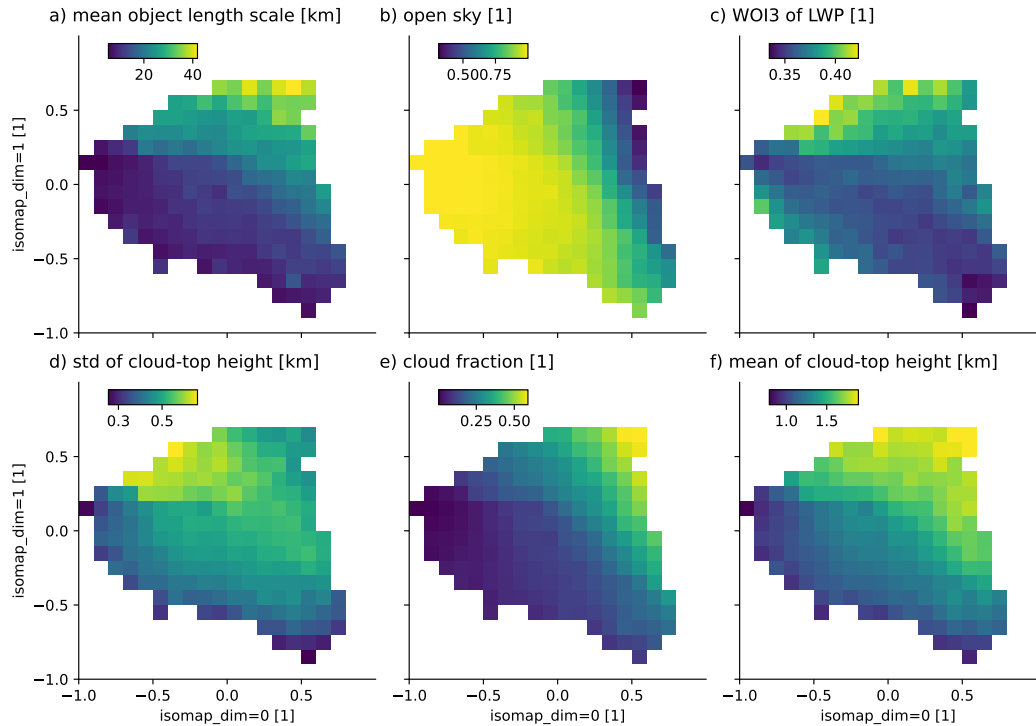


Figure 2: Bin-mean values across embedding manifold of conventional cloud-metrics a) characteristic cloud-size (L_c), b) contiguous open-sky fraction (f_{os}), c) directional alignment of liquid water path (a_{LWP}), d) standard deviation of cloud-top height σ_{CTH} , e) cloud-fraction (f_c) and f) cloud-top height (z_{CTH})

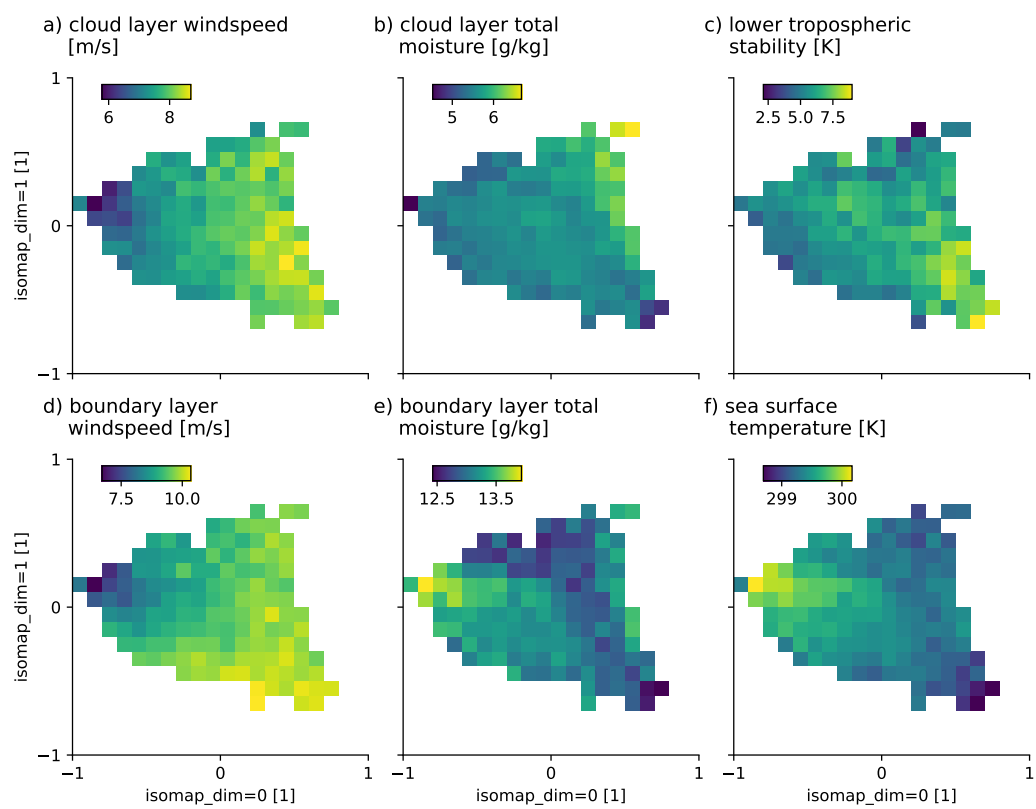


Figure 3: Bin-mean values of environmental characteristics derived from ERA5 reanalysis across the embedding manifold

level moisture (Figure 3e and 3b), with higher cloud-level and lower sub-cloud moisture in the latter case. In fact, the moisture and wind-speed appear nearly orthogonal in their variation across the embedding manifold, so that for contours of fixed moisture, the wind-speed uniquely defines a location on the manifold and thus the kind of organisation typically associated with these conditions. In contrast to B21 and S21, we do not find the strongest stability conditions (Figure 3c) to be associated with large and deep isolated clouds, but rather with the strongest degree of cellular organisation.

3.4 Finding Sugar, Fish, Flowers and Gravel

We next turn to examining the extent to which the convective organisation classes (*Sugar*, *Gravel*, *Fish* and *Flowers*) described by B19 appear as distinct regions on the embedding manifold, examining whether the self-supervised neural network has "discovered" these manually defined classes of organisation. This is done by producing embeddings with the trained neural network at the same locations which have been manually labelled as belonging to one of the four classes and, for each of the four classes in turn, plotting the distribution of these embeddings over the manifold (see Figure 4), thereby showing where the trained neural network would place a tile with a given manual classification. The manually-labelled dataset produced for the EUREC4A field campaign Stevens et al. (2021) by Schulz (2022) containing at $0.01^\circ \times 0.01^\circ$ resolution, for 7/1/2020 to 2/3/2022 in the tropical Atlantic, the number of people labelling a given location in the four classes.

As Schulz (2022) any location with over 60% agreement in labelling is designated as belonging to a specific class. The per-class distribution is visualised by the 50% density contour (showing the spread) and then 90% density contour (containing the peak) computed using Kernel Density Estimation (KDE).

The distribution of tiles labelled as *Sugar*, *Gravel* and *Flowers* peak in distinct regions of the embedding manifold suggesting these three classes of organisation have distinctive characteristics identifiable using unsupervised learning (in contrast to *Fish*, discussed below). The spatial regions labelled *Sugar* are concentrated in the region of the embedding space where scattered isolated cumuli with low vertical extent are concentrated, *Gravel* is associated with (often multi-) cellular cloud structures formed by cold-pool arcs, and *Flowers* in the region of larger, deeper isolated cumuli, all in agreement with B19.

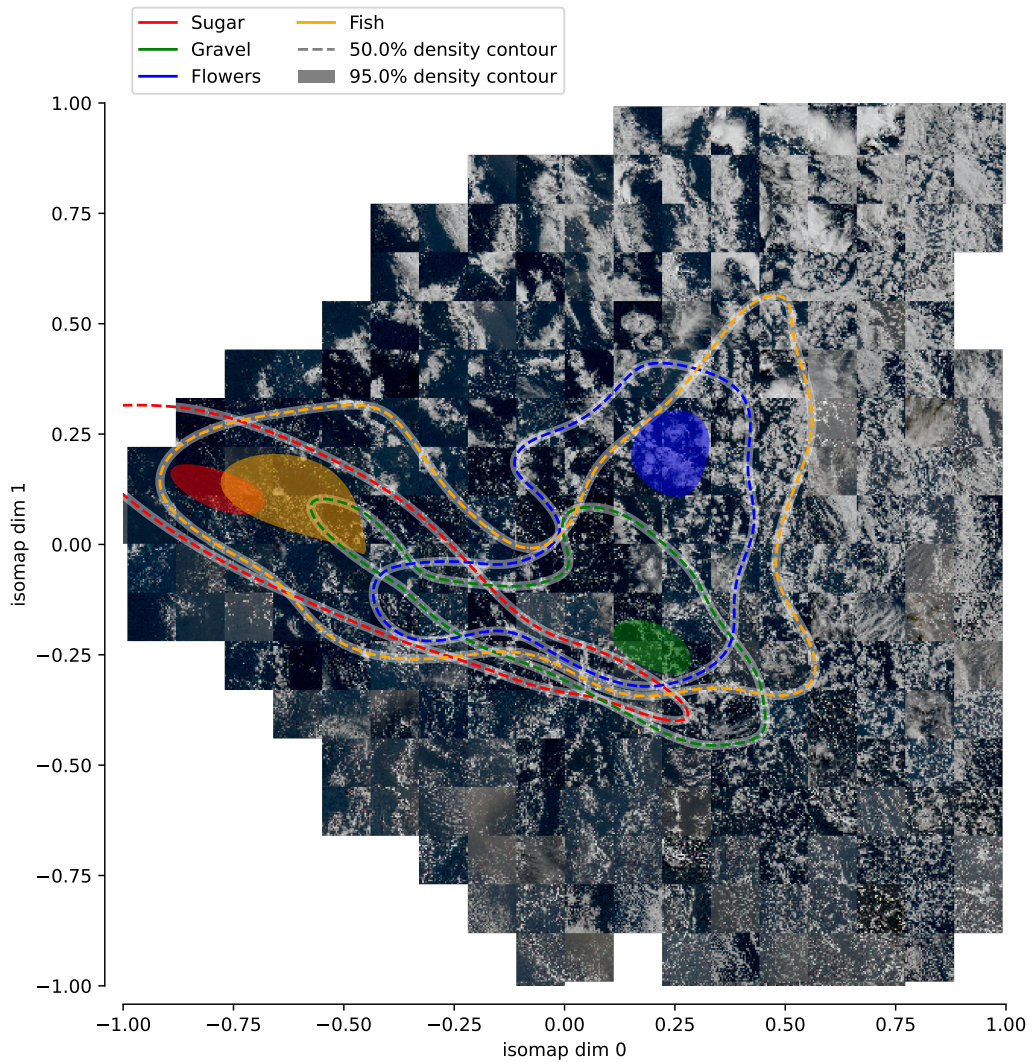


Figure 4: Per-class distribution across the manifold in Figure 1 of embeddings produced by trained neural network of tiles sampled the manually-labelled *Sugar*, *Gravel*, *Flowers* and *Fish* classes of organisation. from across embedding manifold, showing where on the embedding manifold points that were classified as either SGFF fall

However, although the distributions of these three classes peak in isolated regions in embedding manifold, they also show a broad and varying overlap between organisation classes. The *Sugar* class appears the most separated from the rest, fitting with it being the archetypical organisation comprising randomly scattered small shallow cumuli. *Gravel* organisation extends into the region of *Sugar*, fitting with *Gravel* being characterised by cloud-free voids (driven by cold-pools) within regions of shallow scattered cumuli. For tiles labelled as *Flower* organisation, the distribution extends to encompass the peak of the *Gravel* cloud distribution, which is consistent with these larger isolated clouds in some cases being associated with cold-pool arcs. Finally, we consider the distribution of tile samples from regions labelled as *Fish* which is concentrated in same part of the embedding manifold as the *Sugar* class and extends to include all three of the other classes. We conjecture that this is happening due to the large characteristic length-scale of *Fish* organisation (visually often $O(1000\text{km})$). Specifically, on the length-scale of tile-size used in this work it appears that *Fish* organisation is comprised from smaller patterns of mesoscale organisation rather than being distinct.

As mentioned above, the overlaps in the distribution across the embedding manifold of regions manually labelled as belonging to separate kinds of organisation can to some degree be explained by the fact that some kinds of mesoscale cloud structures could be expected to occur together based on physical mechanisms expected to be associated with their formation. The isolated nature of the peaks of the manifold distribution of the three *Sugar*, *Gravel* and *Flower* classes above supports findings of (Stevens et al., 2019) that these kinds of organisation have distinct characteristics. However, looking across all tiles these same classes do not show up as isolated distributions across the embedding manifold. Said another way, these three classes of organisation should be considered as useful waymarkers in the full continuous state-space of mesoscale convective organisation, rather than defining the only distinct kinds of organisation to which most kinds of shallow cumulus cloud formations belong.

3.5 Radiative impact of mesoscale organisation

The principal reason for being interested in convective organisation is the possible impact of organisation of shallow convective clouds on Earth's radiation budget. Using the four classes of organisation by S19, B21 concluded that "*for a given low-cloud amount [we] did not find a significant effect of cloud organisation on the shortwave albedo.*"

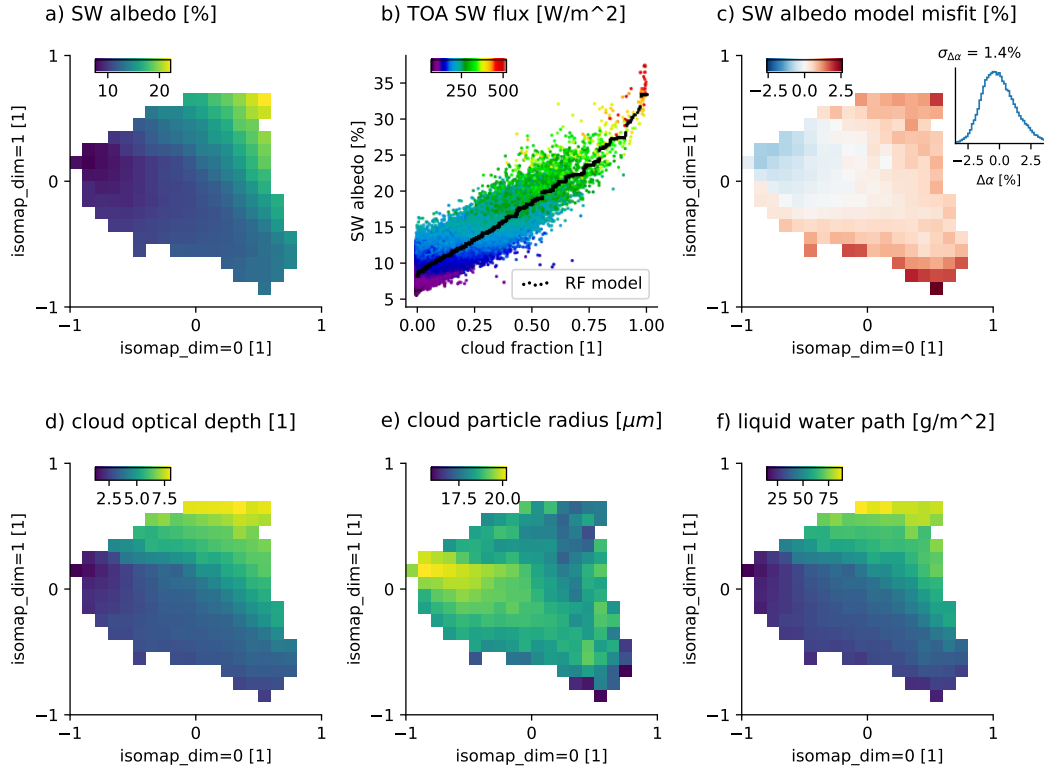


Figure 5: Variation of shortwave albedo a) across the embedding manifold, with cloud-fraction based model miss-fit both b) point-wise and c) across the manifold (distribution in inset) showing the effect of organisation alone (discarding cloud-fraction) together with cloud properties affecting albedo d), e) and f)

From B21 it is clear that to leading-order that mesoscale albedo is controlled by cloud-fraction, however, as the four regimes of organisation studied show little overlap in cloud-fraction, we find it difficult to conclude how strong the effect of organisation is for a given cloud-fraction. To test this conclusion, we here attempt to separate the effect of cloud-fraction and organisation on albedo.

We do this by first fitting a simple model (a random forest, in effect an optimal-binning algorithm producing step-wise predictions) to predict the tile-mean shortwave albedo (Figure 5a) from the tile cloud-fraction. The result of this fit can be seen in Figure 5b) and shows the same monotonic increase in albedo with cloud-fraction as B21. The figure also highlights the significant spread in albedo for a given cloud-fraction (Figure 2e). We next plot the mean error of this simple model across the embedding manifold (Figure 5c), thereby getting a direct visualisation of the extent to which organisation alone affects albedo. In contrast to B21, we do find that organisation effects the shortwave albedo besides through the change of cloud-fraction, with the model albedo miss-fit of $\sigma_{\Delta\alpha} \approx 1.4\%$.

To set the effect of organisation on radiation in context we have included in Figure 5d, 5e and 5f, the mean optical depth, cloud particle radius and liquid water path respectively. Organisation dominated by small scattered cumuli has an anomalously low albedo (compared to what would be predicted from cloud-fraction alone) appearing to result from low cloud optical depth, which in turn results from larger drops and lower total amount of liquid water than other states of organisation across the manifold. In contrast, regimes with higher albedo generally have smaller droplets and higher liquid water path (in cellular organisation) or very small droplets and high liquid water path (large isolated cumuli).

The assumption that cloud organisation only effects the amount of reflected shortwave through changes in cloud-fraction, is in effect assuming that all shallow convective cloudy pixels have the same albedo and the only important factor is how many pixels contain cloud. We have shown here that properties of the cloudy pixels do indeed effect albedo, and the connection between mesoscale organisation and reflected shortwave radiation is more than just cloud-fraction. To fully unpick the role of cloud-properties changing with organisation, further work should be done with in-situ observations and modelling studies to compliment the remote-sensing retrievals used here.

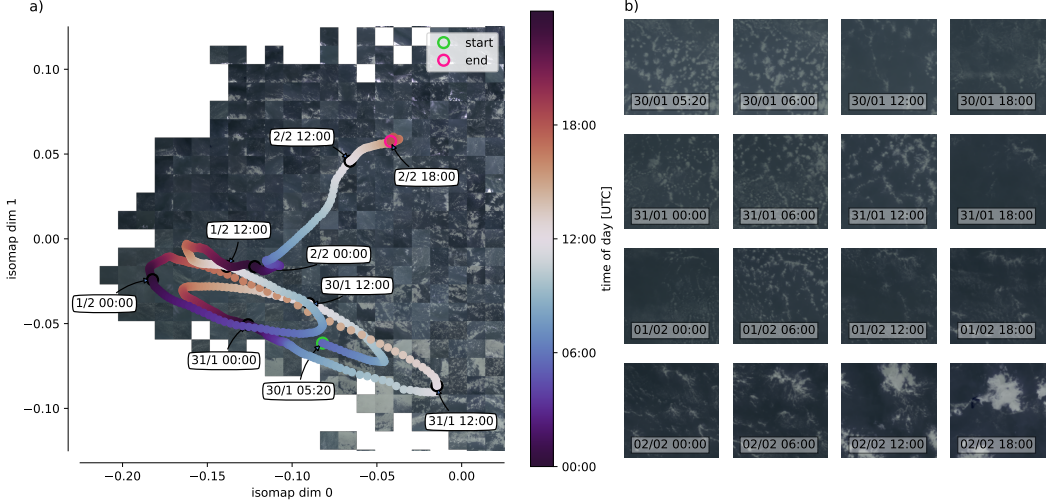


Figure 6: Evolution of cloud organisation along 4-day Lagrangian trajectory arriving at Barbados on 2nd Feb 2020 visualised a) on the embedding manifold and b) with tile samples along the trajectory using IR-tiles (note manifold is different to Figure 1 which is created from model trained on RGB-tiles).

3.6 Mapping the temporal evolution of organisation

In the final use of the embedding manifold we demonstrate how it can be used to study the temporal evolution of cloud organisation. By applying the trained neural network on tiles sampled along a trajectory that follow clouds as they evolve, we can map out transitions between organisational states and thereby investigate the drivers behind these transitions. We use a 4-day trajectory (created with *lagtraj*, Denby & Boeing, 2022), which follows a cloud-layer airmass across the Atlantic as organisation develops from initial isolated scattered cumuli (*Sugar*) into larger isolated cumuli (*Flowers*) (August 2nd 2020, studied by Saffin et al., 2023b; Narenpitak et al., 2021b). Tiles along the trajectory (examples in Figure 6b) are then mapped onto the embedding manifold (Figure 6a). The evolution on the manifold clearly shows, as is also indicated by the tile samples shown, that over the first three days organisation exhibits diurnal cycling that is eventually broken overnight ending in a drastically different regime on February 2nd. In future work this form of manifold trajectory analysis will be used to unpick the mechanisms behind this bifurcation behaviour.

4 Conclusions

In this work we have demonstrated that a map of all possible states of mesoscale organisation exists as an emergent property of the internal embedding space used by an unsupervised neural network, trained to group tiles of similar cloud patterns together.

Examining this embedding manifold map we find that across the manifold the visual variation in cloud patterns matches values of traditional metrics used to measure clouds. Although we find that traditional metrics used for measuring organisation are able to capture the continuum of organisation variation, their varying co-linearity may make them challenging to use in isolation to understand processes of mesoscale organisation. We find that the unsupervised neural network "redisCOVERS" three (*Sugar*, *Flowers* and *Gravel*) of the four classes of organisation defined by Stevens et al. (2019), demonstrated by well-separated peaks in their manifold distribution. However, rather than appearing as isolated regions, these classes appear as useful waymarkers in the full map of cloud organisation produced in this work. By compositing ERA5 reanalysis onto the embedding manifold we find broad agreement with prior work in stronger winds and lower sea-surface temperature being associated with more cellular organisation. However, we also find that the larger isolated clouds are principally found in conditions with high cloud-level and low sub-cloud moisture (rather than lower tropospheric stability being key). Using the continuum representation of organisation we are able to show that cloud organisation *does* affect shortwave albedo beyond simply controlling cloud-fraction. We find that, as expected, this is primarily due to changes in the optical depth, the drivers of which can now be examined using the manifold of organisation. And finally, we have demonstrated how the ability to represent and measure the continuum of organisation allows for the study of how convective organisation develops; examining the evolution of *Sugar* (scattered small cumuli) to *Flowers* (larger isolated cumuli) and capturing the breakaway from diurnal cycling in organisation.

With the urgency of increased capacity to model Earth's future climate, this novel technique to produce a *map* of all states of convective organisation provides a new avenue for how to understand the processes of cloud organisation, both in models and observations, and paves the way for better representation in simulations of Earth's climate.

Acknowledgments

The author acknowledges funding from the Paracon GENESIS (NERC NE/N013840/1) and EUREC⁴A-UK (NERC NE/S015868/1) projects. GOES-16 data is available on the Amazon Open Data Registry at <https://registry.opendata.aws/noaa-goes/>. The Synoptic Radiative Fluxes and Clouds data sets (SYN1deg-1Hour_Terra-Aqua, Edition 4A, https://doi.org/10.5067/TERRA1HOUR_L3.004A and CER_GEO_Ed4_GOE16_NH_V01.2 https://doi.org/10.5067/GOES16/CERES/GEO_ED4_NH_V01.2) are made available by the NASA CERES group.

References

Alinaghi, P., Janssens, M., Choudhury, G., Goren, T., Siebesma, A. P., & Glassmeier, F. (2023). *Shallow cumulus cloud fields are optically thicker when they are more clustered*. doi: <https://doi.org/10.48550/arXiv.2309.08346>

Antonissen, C. (2019). *Organization of Cumulus Convection over (sub) tropical oceans* (Doctoral dissertation). Retrieved from <https://repository.tudelft.nl/islandora/object/uuid{\%}3Ad868273a-b028-4273-8380-ff1628ecabd5>

Bony, S., & Dufresne, J. L. (2005). Marine boundary layer clouds at the heart of tropical cloud feedback uncertainties in climate models. *Geophysical Research Letters*, 32(20), 1–4. doi: 10.1029/2005GL023851

Bony, S., Dufresne, J. L., Le Treut, H., Morcrette, J. J., & Senior, C. (2004). On dynamic and thermodynamic components of cloud changes. *Climate Dynamics*, 22(2-3), 71–86. doi: 10.1007/s00382-003-0369-6

Bony, S., Schulz, H., Vial, J., & Stevens, B. (2020). Sugar, gravel, fish, and flowers: Dependence of mesoscale patterns of trade-wind clouds on environmental conditions. *Geophysical research letters*, 47(7), e2019GL085988.

Bony, S., Stevens, B., Frierson, D. M. W., Jakob, C., Kageyama, M., Pincus, R., ... Webb, M. J. (2015). Clouds, circulation and climate sensitivity. *Nature Geoscience*, 8(4), 261–268. Retrieved from <http://dx.doi.org/10.1038/ngeo2398> doi: 10.1038/ngeo2398

Brune, S., Buschow, S., & Friederichs, P. (2021). The local wavelet-based organization index – Quantification, localization and classification of convective organization from radar and satellite data. *Quarterly Journal of the Royal Meteorological Society*, 147(736), 1853–1872. doi: 10.1002/qj.3998

Dauhut, T., Couvreux, F., Bouniol, D., Beucher, F., Volkmer, L., Pörtge, V., ...

Wirth, M. (2023). Flower trade-wind clouds are shallow mesoscale convective systems. *Quarterly Journal of the Royal Meteorological Society*, 149(750), 325-347. Retrieved from <https://rmets.onlinelibrary.wiley.com/doi/abs/10.1002/qj.4409> doi: <https://doi.org/10.1002/qj.4409>

Denby, L. (2020, jan). Discovering the Importance of Mesoscale Cloud Organization Through Unsupervised Classification. *Geophysical Research Letters*, 47(1). Retrieved from <https://onlinelibrary.wiley.com/doi/10.1029/2019GL085190> doi: 10.1029/2019GL085190

Denby, L., & Boeing, S. (2022). *Eurec4a-uk/lagtraj: v0.1.2*. Zenodo. Retrieved from <https://zenodo.org/record/7506620> doi: 10.5281/ZENODO.7506620

Denby, L., & Janssens, M. (2022, aug). *cloudsci/cloudmetrics: v0.2.0*. Zenodo. Retrieved from <https://doi.org/10.5281/zenodo.7506966> doi: 10.5281/zenodo.7506966

Hersbach, H., Bell, B., Berrisford, P., Hirahara, S., Horányi, A., Muñoz-Sabater, J., ... Thépaut, J.-N. (2020). The era5 global reanalysis. *Quarterly Journal of the Royal Meteorological Society*, 146(730), 1999-2049. Retrieved from <https://rmets.onlinelibrary.wiley.com/doi/abs/10.1002/qj.3803> doi: <https://doi.org/10.1002/qj.3803>

Janssens, M., Vilà-Guerau de Arellano, J., Scheffer, M., Antonissen, C., Siebesma, A. P., & Glassmeier, F. (2021, mar). Cloud Patterns in the Trades Have Four Interpretable Dimensions. *Geophysical Research Letters*, 48(5), 1-14. Retrieved from <https://onlinelibrary.wiley.com/doi/10.1029/2020GL091001> doi: 10.1029/2020GL091001

Kurihana, T., Foster, I., Willett, R., Jenkins, S., Koenig, K., Werman, R., ... Moyer, E. (2022). *Cloud classification with unsupervised deep learning*. arXiv. Retrieved from <https://arxiv.org/abs/2209.15585> doi: 10.48550/ARXIV.2209.15585

Kurihana, T., Moyer, E., Willett, R., Gilton, D., & Foster, I. (2022). Data-driven cloud clustering via a rotationally invariant autoencoder. *IEEE Transactions on Geoscience and Remote Sensing*, 60, 1-25. Retrieved from <https://doi.org/10.1109/TGRS.2021.3098008> doi: 10.1109/tgrs.2021.3098008

Kurihana, T., Moyer, E. J., & Foster, I. T. (2022, nov). AICCA: AI-driven cloud classification atlas. *Remote Sensing*, 14(22), 5690. Retrieved from <https://doi.org/10.3390/rs14225690>

.org/10.3390%2Frs14225690 doi: 10.3390/rs14225690

Medeiros, B., Stevens, B., Held, I. M., Zhao, M., Williamson, D. L., Olson, J. G., & Bretherton, C. S. (2008). Aquaplanets, climate sensitivity, and low clouds. *Journal of Climate*, 21(19), 4974–4991. doi: 10.1175/2008JCLI1995.1

Muller, C., Yang, D., Craig, G., Cronin, T., Fildier, B., Haerter, J. O., ... others (2022). Spontaneous aggregation of convective storms. *Annual Review of Fluid Mechanics*, 54, 133–157.

Narenpitak, P., Kazil, J., Yamaguchi, T., Quinn, P., & Feingold, G. (2021a). From sugar to flowers: A transition of shallow cumulus organization during atomic. *Journal of Advances in Modeling Earth Systems*, 13(10), e2021MS002619. Retrieved from <https://agupubs.onlinelibrary.wiley.com/doi/abs/10.1029/2021MS002619> (e2021MS002619 2021MS002619) doi: <https://doi.org/10.1029/2021MS002619>

Narenpitak, P., Kazil, J., Yamaguchi, T., Quinn, P., & Feingold, G. (2021b, oct). From sugar to flowers: A transition of shallow cumulus organization during ATOMIC. *Journal of Advances in Modeling Earth Systems*, 13(10). Retrieved from <https://doi.org/10.1029/2F2021ms002619> doi: 10.1029/2021ms002619

NASA/LARC/SD/ASDC. (2017, 9 19). *Ceres and geo-enhanced toa, within-atmosphere and surface fluxes, clouds and aerosols 1-hourly terra-aqua edition4a*. NASA Langley Atmospheric Science Data Center DAAC. Retrieved from https://doi.org/10.5067/TERRA+AQUA/CERES/SYN1DEG-1HOUR_L3.004A

NASA/LARC/SD/ASDC. (2018, 8 8). *Satcorps ceres geo edition 4 goes-16 northern hemisphere version 1.2*. NASA Langley Atmospheric Science Data Center DAAC. Retrieved from https://doi.org/10.5067/GOES16/CERES/GEO_ED4_NH_V01.2

Saffin, L., Lock, A., Tomassini, L., Blyth, A., Böing, S., Denby, L., & Marsham, J. (2023a). Kilometer-scale simulations of trade-wind cumulus capture processes of mesoscale organization. *Journal of Advances in Modeling Earth Systems*, 15(3), e2022MS003295. Retrieved from <https://agupubs.onlinelibrary.wiley.com/doi/abs/10.1029/2022MS003295> (e2022MS003295 2022MS003295) doi: <https://doi.org/10.1029/2022MS003295>

Saffin, L., Lock, A., Tomassini, L., Blyth, A., Böing, S., Denby, L., & Marsham, J. (2023b, mar). Kilometer-scale simulations of trade-wind cumulus capture processes of mesoscale organization. *Journal of Advances in Modeling Earth Sys-*

tems, 15(3). Retrieved from <https://doi.org/10.1029/2022ms003295> doi: 10.1029/2022ms003295

Schulz, H. (2022). C3ONTEXT: A Common Consensus on Convective OrgaNizaTion during the EUREC4A eXperiment. *Earth System Science Data*, 14(3), 1233–1256. doi: 10.5194/essd-14-1233-2022

Schulz, H., Eastman, R., & Stevens, B. (2021). Characterization and Evolution of Organized Shallow Convection in the Downstream North Atlantic Trades. *Journal of Geophysical Research: Atmospheres*, 126(17), 1–18. doi: 10.1029/2021JD034575

Stevens, B., Bony, S., Brogniez, H., Hentgen, L., Hohenegger, C., Kiemle, C., ... Zuidema, P. (2019). Sugar, Gravel, Fish, and Flowers – Mesoscale cloud patterns in the Tradewinds. *Quarterly Journal of the Royal Meteorological Society*.

Stevens, B., Bony, S., Farrell, D., Ament, F., Blyth, A., Fairall, C., ... Zöger, M. (2021). Eurec4a. *Earth System Science Data*, 13(8), 4067–4119. doi: 10.5194/essd-13-4067-2021

Tenenbaum, J. B., de Silva, V., & Langford, J. C. (2000, dec). A global geometric framework for nonlinear dimensionality reduction. *Science*, 290(5500), 2319–2323. Retrieved from <https://doi.org/10.1126/science.290.5500.2319> doi: 10.1126/science.290.5500.2319

Vial, J., Dufresne, J. L., & Bony, S. (2013). On the interpretation of inter-model spread in CMIP5 climate sensitivity estimates. *Climate Dynamics*, 41(11-12), 3339–3362. doi: 10.1007/s00382-013-1725-9

Webb, M. J., Senior, C. A., Sexton, D. M., Ingram, W. J., Williams, K. D., Ringer, M. A., ... Taylor, K. E. (2006). On the contribution of local feedback mechanisms to the range of climate sensitivity in two GCM ensembles. *Climate Dynamics*, 27(1), 17–38. doi: 10.1016/j.pbiomolbio.2006.02.004

Wing, A. A., Emanuel, K., Holloway, C. E., & Muller, C. (2018). Convective self-aggregation in numerical simulations: A review. *Shallow clouds, water vapor, circulation, and climate sensitivity*, 1–25.